Vol. 14, No. 1, 96-110, https://doi.org/10.22712/susb.20230008

INTERNATIONAL JOURNAL OF
SUSTAINABLE Building Technology and Urban Development

pISSN 2093-761X · eISSN 2093-7628

Development of hybrid chitosan/zinc oxide/graphene oxide nanocomposites for potential food packaging application

Dhiren Kanted[1], Vishnu Soman[2], Simran Sahota[1] and Maneesh Kumar Poddar[3*]

[1]Post Graduate Student, Department of Chemical Engineering, National Institute of Technology Karnataka Surathkal, India
[2]Research Scholar, Department of Chemical Engineering, National Institute of Technology Karnataka Surathkal, India
[3]Assistant Professor, Post Graduate Student, Department of Chemical Engineering, National Institute of Technology Karnataka Surathkal, India

***Corresponding author:** maneesh.poddar@nitk.edu.in

Received: 10 February 2022
Accepted: 12 January 2023

A B S T R A C T

Novel food packaging materials are becoming increasingly necessary and extensive research is underway worldwide towards developing environmentally friendly and bio-based polymers. Among various biopolymers, chitosan is the noticeable and industrially viable food packaging material and is the second most naturally available biopolymer after cellulose. This study is based on the reinforcing hybrid nanomaterials of zinc and graphene oxides into the chitosan matrix to produce a bio-based food packaging material with improved antimicrobial properties, high water resistance and thermally stable hybrid chitosan/ZnO/GO nanocomposites. Various characterization techniques such as Raman, FTIR, XRD and FE-SEM confirmed the preparation of nanofillers and their successful encapsulation into the chitosan matrix. The thermal analysis results confirmed a marked rise of 46.5 and 62.1°C at $T_{25\%}$ and $T_{50\%}$ respectively of hybrid nanocomposites as compared to neat chitosan. Further, the DTG analysis showed there was a significant rise of 19°C in the maximum degradation temperature for hybrid chitosan/ZnO/GO nanocomposites as compared to neat chitosan. The water vapor permeability of hybrid nanocomposites was reported at a minimum of 1.04 g.mm/m^2.h.kPa against the neat chitosan of 2.22 g.mm/m^2.h.kPa which confirmed the nanocomposites with improved water resistance. The antimicrobial property tested in presence of *Bacillus subtilis* (gram-positive bacterium) was reported maximum for hybrid chitosan/ZnO/GO nanocomposites with the highest inhibition zone of 12 mm as compared to the inhibition zone of neat chitosan, chitosan/GO, and chitosan/ZnO of 5 and 10 mm respectively. The increase in the above properties of the hybrid nanocomposites is attributed to the combined effect of hybrid nanofillers as compared to the nanocomposites with the use of single nanofillers.

Keywords: chitosan; zinc oxide; graphene oxide; hybrid nanocomposites; food packaging

Introduction

Polymers are being extensively used as food packaging materials due to their inert behavior against atmospheric oxygen and moisture, low cost, lightweight, and ease of production. Synthetic polymers derived from petrochemical sources, such as polypropylene, polystyrene, polyethylene, PTFE terephthalate, and others, are non-biodegradable,

and their continuous accumulation generates excessive solid waste, which has become a major global concern for the environment and ecosystem. Replacing synthetic polymers with bio-based or biodegradable kinds is an alternate and environmentally beneficial way to overcome this problem [1-4]. Food packaging materials made of biodegradable or bio-based polymers can be degraded while in contact with the micro-organisms present in the environment [5].

Chitosan is a polysaccharide that is the second most abundant biopolymer on the planet. Chitin is a crucial component of crustacean and insect exoskeletons, as well as yeast and fungal cell walls. It is widely utilised in food packaging applications due to its non-toxic, non-allergic, and antibacterial qualities. The antibacterial capabilities of neat chitosan are limited, and it is a poor water vapour barrier. As a result, the diffusion of atmospheric moisture through food packing materials comprised of near chitosan leads to microbial contamination. Furthermore, chitosan's low thermal stability prevents it from being used to pack high-temperature foods. The thermal analysis investigation revealed that biopolymers had poor thermal stability at temperatures above 200°C, limiting their applicability [6-8].

The addition of nanofillers to the chitosan matrix, referred to as "chitosan nanocomposites," improves thermal stability, water vapour resistance, and antibacterial activity [9]. A recent work discovered that incorporating silver nanoparticles in chitosan matrix improved the antibacterial properties of chitosan/Ag nanocomposites [10, 11]. Another study found that encapsulating inorganic metal oxides improved the thermal stability and antibacterial characteristics of pristine chitosan [12]. Antimicrobial and photocatalytic characteristics of metal oxides are well established. Because of its white colour, high antibacterial activity, and excellent water barrier qualities, zinc oxide (ZnO) is frequently utilised as a food additive and food packaging material [13]. However, its thermal stability is reduced.On the other hand, graphene oxide (GO) is known to be an excellent disinfectant agent against a wide range of pathogenic microbes, as well as having high thermal stability and excellent mechanical properties due to the presence of various functional groups such as epoxy, carboxyl, and hydroxyl at the ends of graphene oxide sheets, and its composites with chitosan can further improve the thermal stability and other physical properties of chitosan nanocomposites [14]. Hybrid nanocomposites are the subject of extensive research, since the integration of several types of nanofillers has resulted in a significant improvement in the physical properties of the neat polymer. Previous studies showed the preparation of chitosan/organomodified-montmorillonite/Thyme oil samples had 53 percent more antioxidant activity than Chitosan/sodium−montmorillonite/Thyme oil samples [15]. These experiments indicated that such films exhibited a decreased value of Thiobarbituric acid reactive substances (TBARS) than commercial LDPE and neat chitosan films. The addition of lignin nanoparticles (NPS) into chitosan/PVA hydrogels enabled water accessibility into the amorphous regions of the hydrogels [16]. The antioxidative response by DPPH activity of migrated substances revealed the synergistic effect of CS and lignin nanoparticles. Also, the lignin nanoparticles were found to have profound effects against gram-negative bacteria, namely *Escherichia coli*. Incorporation of ZnO showed an increase in tensile modulus and tensile strength of film by 77% and 67%, respectively at 2% ZnO NPs concentration. The increase in ZnO concentration resulted in the

enhancement of the antimicrobial activity by 2 times and 1.5 times respectively in *Bacillus subtilis and Escherichia coli*. [17]. The synthesis of chitosan-carboxymethyl cellulose composite films by incorporating cinnamon essential oil (CEO), oleic acid (OA), and glutaraldehyde (GL) has shown a reduction in film water solubility by 27%, 38%, and 16%, respectively [18]. It is also reported that three varied types of sulfur nanoparticles (SNP) to prepare functional CS/SNP composite films. SNP addition enhanced the mechanical and water vapour barrier (WVB) properties of the composite film in addition to exhibiting a distinctive UV light screening effect without compromising the film transparency. The residual char content at 600°C of the neat chitosan, chitosan/SNP1, chitosan/SNP2, and chitosan/SNP3 composite films were 33.0, 38.9, 34.1, and 39.5%, respectively, indicating an increase in thermal stability of the film increased blending with the SNPs [19]. The addition of a single nanofiller of ZnO into the chitosan matrix can impart mainly antibacterial and water barrier properties but at the cost of compromised thermal stability. However, the thermal stability of chitosan can be augmented with the encapsulation of GO into the chitosan matrix with moderate improvement in antibacterial and water barrier properties of the final chitosan nanocomposites. It has been always difficult to improve all the above-desired properties of neat chitosan using single nanofillers. Therefore, in this current work, we aim to improve all the desired properties using hybrid nanofillers. This synthesis method is essentially used to evaluate the individual and combined effect of both nanofillers for antimicrobial, thermal, and water barrier properties of chitosan/ZnO/GO nanocomposites for increasing the food shelf life.

Material and Methodology

Materials

Chitosan powder (medium molecular weight) with 90% degree of deacetylation, zinc acetate dihydrate and acetic acid were purchased from SRL chemicals, India. The chemicals namely hydrogen peroxide 30% (w/v), potassium permanganate (KMnO4), hydrochloric acid (HCl), sulphuric acid (H_2SO_4), phosphoric acid (H_3PO_4) and sodium hydroxide (NaOH) in pellet form were procured from Merck, India. Graphite fine powder was obtained from Loba chemicals, India. The strains of *Bacillus subtilis* were obtained from National Centre for Industrial Microorganisms-Pune, India. The reagents procured were of analytical grade and hence no additional purification was required. The solutions used during the entire experiment were prepared using ultra-pure water.

Synthesis of Nanofillers

Synthesis of ZnO

Zinc oxide (ZnO) nanoparticles were synthesized using zinc acetate dihydrate (Zn $(CH_3COO)_2.2H_2O$) and sodium hydroxide (NaOH) by using the sol-gel method [20]. In this, 25 ml of 0.2 M stock solutions of zinc acetate dihydrate were mixed in 50 ml methanol with continous stirring until a homogenous solution was obtained. Further, 50 ml of NaOH (0.2 M) as prepared in ultra-pure water was added into Zn $(CH_3COO)_2.2H_2O$ (0.2 M) stock

solutions under constant stirring. The reaction was performed at 5 ± 1°C by using an ice bath at the periphery of the flask. The reaction oxidized Zn $(CH_3COO)_2.2H_2O$ into white suspension of zinc oxide (ZnO) nanoparticles. This suspension was left overnight and allowed to settle the ZnO. After this, the supernatant was discarded and the remaining suspension was filtered out using Whatman filter paper. The white filtrate of ZnO nanoparticles was further washed using a mixture of ethanol and deionized water to eliminate any impurities present in it. After washing, the final filtrate was dried in a hot air oven at 70°C for 36 h. Followed by drying, the ZnO nanoparticles were stored in the desiccator and further used for characterization and nanocomposites preparation.

Synthesis of Graphene Oxide

The Tour's method, which is a modified version of the well-known Hummer's method [21], was used to synthesise graphene oxide (GO). Initially, 30 ml of concentrated sulphuric acid was mixed with 3.3 ml of concentrated phosphoric acid and the mixture was magnetically stirred in an ice bath for 30 min. Further, 1.0 g of graphite powder followed by 6 g of $KMnO_4$ was slowly added into the mixture and continued stirring for 30 min. The addition of $KmnO_4$ into the mixture resulted in the oxidization of graphite powder into graphene oxide. The temperature of the reaction mixture was raised to 35°C after 30 min and kept under constant stirring for the next 2 h to ensure complete oxidation. After adding 100 ml ultra-pure water and 10 ml H_2O_2, the oxidation process was stopped, and the colour of the liquid changed from dark brown to golden brown. The oxidised mixture was allowed to settle overnight before the supernatant was discarded. To remove the suspended contaminants, the settled GO mixture was centrifuged (Kubota 6930, Japan) at 6000 rpm for 20 min at 4°C. The supernatant was decanted and the retentate was washed using dilute HCl (1:10 dilution with ultra-pure water). This was followed by drying in a hot air oven set to 85°C for 12 h. After drying, the GO in the form of nanosheets was stored in a desiccator and used for characterization and nanocomposites preparation.

Synthesis of chitosan nanocomposites

The preparation of neat chitosan and its nanocomposites of chitosan/ZnO, chitosan/GO and hybrid chitosan/ZnO/GO was done using the solvent casting method. In this method, 2 g chitosan powder was dispersed in 100 ml of dilute acetic acid solution (1% v/v) and kept under magnetic stirring for 12 h at 70°C. After complete mixing, the homogenous mixture was poured into petri-dish and allowed for evaporation of acetic acid at room temperature. The residual acid that remained in the film was further removed via drying it in a hot air oven at 60°C for 24 h. A similar method for the preparation of chitosan nanocomposites was used and is described as follows. For the preparation of chitosan/ZnO nanocomposites, chitosan powder along with ZnO (2% w/w) was dispersed into dilute acetic acid and magnetically stirred overnight for uniform dispersion of ZnO into chitosan mixture. Overnight mixed dispersion was poured into a Petri dish for film formation as a similar technique was earlier used during film formation of neat chitosan. A similar method for the preparation of chitosan/GO was used via the dispersion of 2.0 wt% GO into chitosan- acetic acid solution. Further, the hybrid film of chitosan/ZnO/GO was prepared via dispersing the individual filler concentration of ZnO and GO each of 1.0 wt% into chitosan- acetic acid solution.

The concentration of individual nanofillers of ZnO and GO was kept at 1.0 wt% to maintain the overall concentration of 2 wt% into the chitosan- acetic acid solution.

Characterization

The Raman spectral analysis of graphite powder and graphene oxide (GO) were performed using the Laser Micro Raman System (Horiba Jobin Vyon, Model: Lab Ram HR) with an excitation wavelength of 488 nm. Fourier transform infrared (FTIR, make-JASCO-4200) spectrometer in ATR mode (attenuated total internal reflection) was used to examine the successful encapsulation of single and hybrid nanofillers into the neat chitosan film. In this, the analysis of various functional groups was performed at room temperature in the range of 4000-400 cm^{-1}. The crystalline structure of graphite powder, GO and nanocomposites were measured using X-ray diffraction (XRD, make-JEOL-JPZ 8). The analysis for ZnO was performed using copper target (Cu -Kα radiation, λ = 1.54 Å) in the 2θ range of 20°-70° and for GO and chitosan nanocomposites were done in 2θ range of 5°to 70° with the scanning rate of 7°/min. The surface morphologies and successful encapsulation of nanofillers into the chitosan matrix were examined using field emission scanning electron microscopy (FESEM, make-JEOL-JSM-6380LA, Tokyo, Japan). Measurement of thermal stability of neat chitosan and its nanocomposites were determined using thermogravimetric analysis (TGA) (NETZSCH TG, Model: 209F1 Libra) at heating rates of 10°C/min in N_2 atmosphere. To estimate water vapor transmission and permeability of the films, the assessment of water vapor permeability was done gravimetrically by a modified ASTM E96 method [22, 23]. Strips of the biopolymer films were cut and sealed on the top of test tubes with 10 ml u water maintained at a relative humidity of 78% and were placed in a laboratory desiccator filled with silica gel as a desiccant. The relative humidity inside the desiccator was maintained at an average of 31%. The humidity was monitored using a digital hygrometer (Testo brand). The weight loss of the testtubes sealed with films was noted daily to the nearest 0.0001 g until the value reached a constant. The values of water vapor transmission rate (WVTR) and water vapor permeability (WVP) for each film were determined using following equations:

$$\text{WVTR}=\frac{\Delta w/t}{A} \tag{1}$$

$$\text{WVP}=\frac{WVTR\times x}{p_w\times(RH_1-RH_2)} \tag{2}$$

Where $\triangle w$/t is the slope of the plot between weight loss against time (g/h) which was estimated using linear regression and A is the exposed area of the film (m^2). x is the film thickness (mm), p_W is the vapor pressure (kPa), RH_1 and RH_2 are the relative humidity (%) inside and outside of the test tubes respectively.

The antibacterial properties of nanocomposites were investigated using the agar well diffusion assay method. The microorganisms used to assess the antimicrobial susceptibility were *Bacillus subtilis* (gram-positive bacterium). The following was the antibacterial testing method: Petriplates were poured with sterile Luria Bertani

(LB) agar medium containing 15 g/L agar-agar and allowed to solidify for a few minutes.Wells of diameter 10 mm were made in the agar plate using a sterile cork borer and the prepared films were inserted into the wells. The plates were inoculated with three overnight grown bacterial cultures prepared beforehand.The plates were placed in a stationary incubator at 37°C for 24 h. The films with antimicrobial properties inhibit *Bacillus subtilis* resulting in a zone of clearance and the diameter of the zone was measured after an incubation period of 24 h. To achieve suitable sterile conditions, the entire antimicrobial study was carried out inside the Laminar airflow hood (model: UH22).

Result and Discussions

Raman spectra of graphite powder and GO are shown in Figure 1. It can be seen from Figure 1, graphite powder exhibits a single and sharp peak at ~ 1585 cm^{-1} that corresponds to the G band and arises due to carbon-carbon bond stretching [24]. After the conversion of graphite into GO, two characteristic peaks at 1355 cm^{-1} (D-band) and 1589 cm^{-1} (G band) are observed. It can be seen that the G band present in GO has shifted towards a higher wavenumber as compared to graphite due to the oxygenation of graphite during the oxidation reaction [25]. The D-band at 1355 cm^{-1} essentially confirms the sp^3 state of a carbon atom in GO and appeared due to the presence of various defects in GO. Also, the D band in GO is a little broader than the G band due to the distortion and defects formation in its sp^3 carbon atoms during the oxidation reaction. The ratio of intensities corresponding to D- and G-bands (ID: IG ratio) which represents the relative population of the sp^3:sp^2 hybridized carbon atoms is found higher in GO (ID: IG ~1.0) as compared to graphite (ID: IG ~ 0.45) and this indicates the increase in defects during the oxidation process.

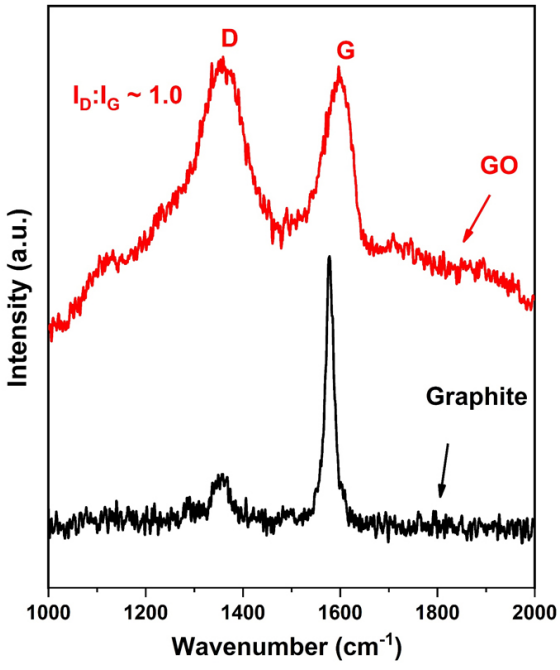

Figure 1. Raman spectra of graphite powder and graphene oxide (GO).

FTIR-ATR spectra of neat chitosan and its single and hybrid nanocomposites with encapsulation of ZnO and GO are shown in Figure 2. Transmittance peaks of neat chitosan present at 2860 and 1020 cm^{-1} correspond to the stretching and bending vibration of hydroxyl groups respectively [26]. Further, the peak at 1550 and 2925 cm^{-1} attributed to the scissoring vibration of $-NH_2$, and C-H stretching into the chitosan [27]. The broad absorption band in the range of 650 − 800 cm^{-1} shows the presence of ZnO in chitosan/ZnO nanocomposites. This broad absorption band is attributed to the stretching vibrations of N − Zn and O − Zn-O [28]. The FTIR-ATR spectra of chitosan/GO with a characteristic peak present at 1260 cm^{-1} attributes to C-O stretching and confirms the presence of GO into nanocomposites. However, in hybrid chitosan/ZnO/GO nanocomposites, the broad absorption band of ZnO in the range of 650-800 cm^{-1} and the characteristic peak of GO at 1260 cm^{-1} are present and confirms the successful encapsulation of hybrid nanofillers into the chitosan matrix. Moreover, the peak intensities in single and hybrid chitosan nanocomposites varied and this is due to the variation in nanofillers concentration into the final nanocomposites. Overall, FTIR analysis has established the successful encapsulation of ZnO and GO nanofillers into the chitosan matrix.

The XRD image of zinc oxide nanoparticles (ZnO NPs) is depicted in Figure 3. The diffraction peaks at 2θ = 31.8, 34.43, 36.18, 47.53, 56.56, 62.89 and 67.86 assigned crystallographic plane values of (110), (002), (101), (102), (110), (103) and (112) respectively. The peaks obtained are in close agreement with JCPDS card no. 5-0664 corresponding to zincite phase. Since no other peaks except for ZnO is present, a pure synthesis can be inferred. The diffractogram hence obtained corresponds to the Hexagonal Zincite phase of ZnO. The average crystallite size depending on the peaks found from XRD was 17.16nm which confirms the synthesis of ZnO on the nanoscale. The XRD patterns of GO, neat chitosan and its nanocomposites with ZnO and GO are shown in Figure 4. GO shows a sharp peak at 2θ =8.8° which indicates a marked rise in interlayer *d*-spacing as compared to graphite molecules

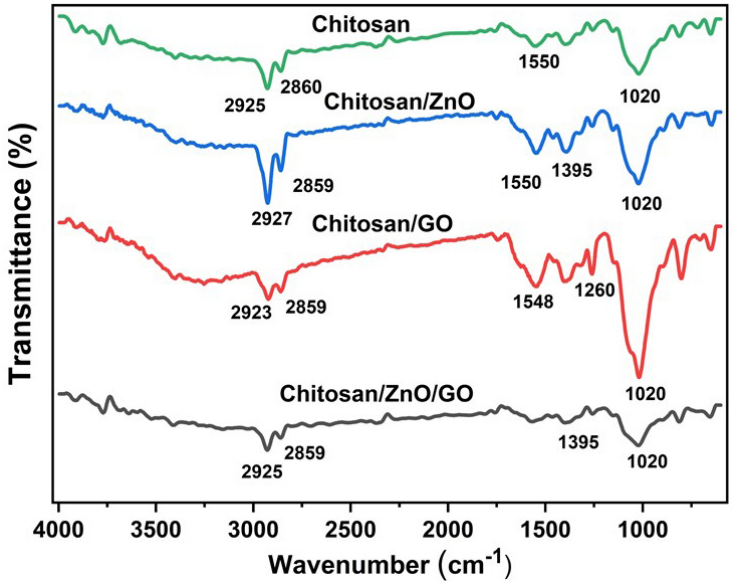

Figure 2. ATR-FTIR spectra of chitosan, chitosan/ZnO, chitosan/GO and chitosan/ZnO/GO nanocomposites.

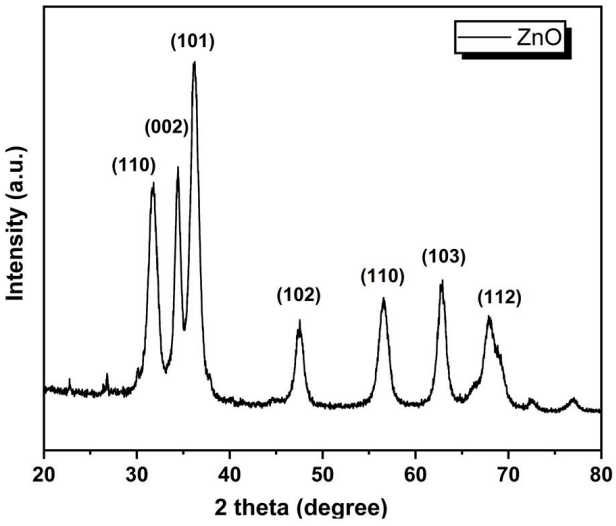

Figure 3. X-ray diffractograms of zinc oxide nanoparticles.

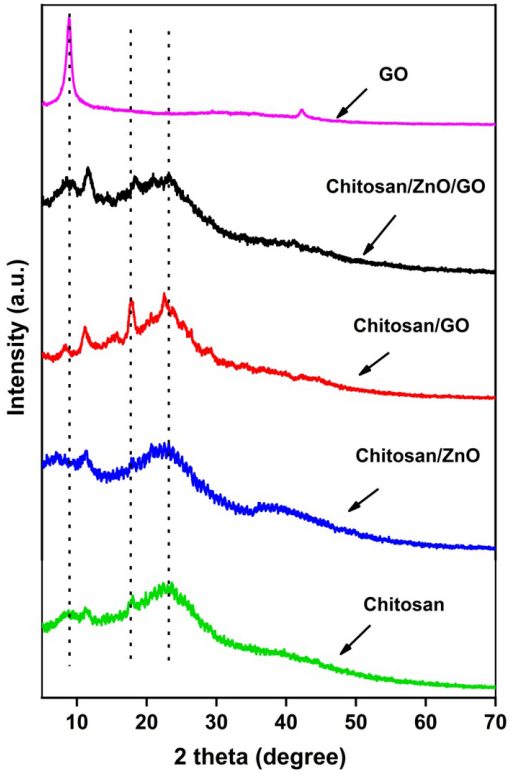

Figure 4. X-ray diffractograms of graphene oxide (GO), chitosan, chitosan/ZnO, chitosan/GO and chitosan/ZnO/GO nanocomposites.

which normally show low *d*-spacing with an intense peak in the 2θ range of 25-30° [24]. The X-ray diffractogram of the neat chitosan shows peaks at around 17.84° and corresponds to the crystalline structure and the broad peak present at 22.38° attributes the amorphous structure of chitosan molecules [29, 30]. XRD diffraction of chitosan/GO shows a sharp and intense peak (a little higher than chitosan) at $2\theta = 8.8°$ which corresponds to the

successful encapsulation of GO into the chitosan matrix. However, the intensity of this peak is smaller than the GO due to the low loading of GO (1 wt%) into the chitosan matrix. Also, new sharp peaks in chitosan/GO at 2θ =11.13, 17.22 and 22.65° are observed and this indicates that the addition of GO into chitosan imparts the crystalline structure in the chitosan/GO nanocomposites. In the case of chitosan/ZnO nanocomposites, additional sharp peaks are also observed but at low intensity, as compared to various sharp peaks of ZnO at different 2θ values. The possible reason for this less intense peak could be the low encapsulation of ZnO into the chitosan matrix. On the other hand, the XRD of hybrid chitosan/ZnO/GO shows numerous additional intense peaks as observed during chitosan/GO nanocomposite but with a reduction in peak intensity. The reduction in peak intensity attributes to the addition of ZnO along with the GO nanofillers into the chitosan matrix.

The FE-SEM micrographs of ZnO, GO nanofillers and chitosan/ZnO nanocomposites were examined and the images are shown in Figure 5. In Figure 5(a), ZnO showed a rod-type configuration while Figure 5(b) shows the graphene oxide (GO) flakes type structure with a relatively large surface area. Figure 5(c) shows a micrograph of neat chitosan film and Figure 5(d) depicts the FE-SEM micrograph of chitosan/ZnO nanocomposites with 1 wt% ZnO loading with the uniform dispersion of ZnO into the chitosan matrix.

The thermal stability behavior of neat chitosan and its single and hybrid nanocomposites with ZnO and GO have been assessed with TGA thermograms, the results of which are shown in Figure 6. The expanded view of TGA curves in the temperature range of 250-600°C is shown in Figure 6(b). The results of these curves with temperature for a weight loss of 10, 25 and 50% are also compiled in Table 1. It is evident from the results for the neat chitosan,

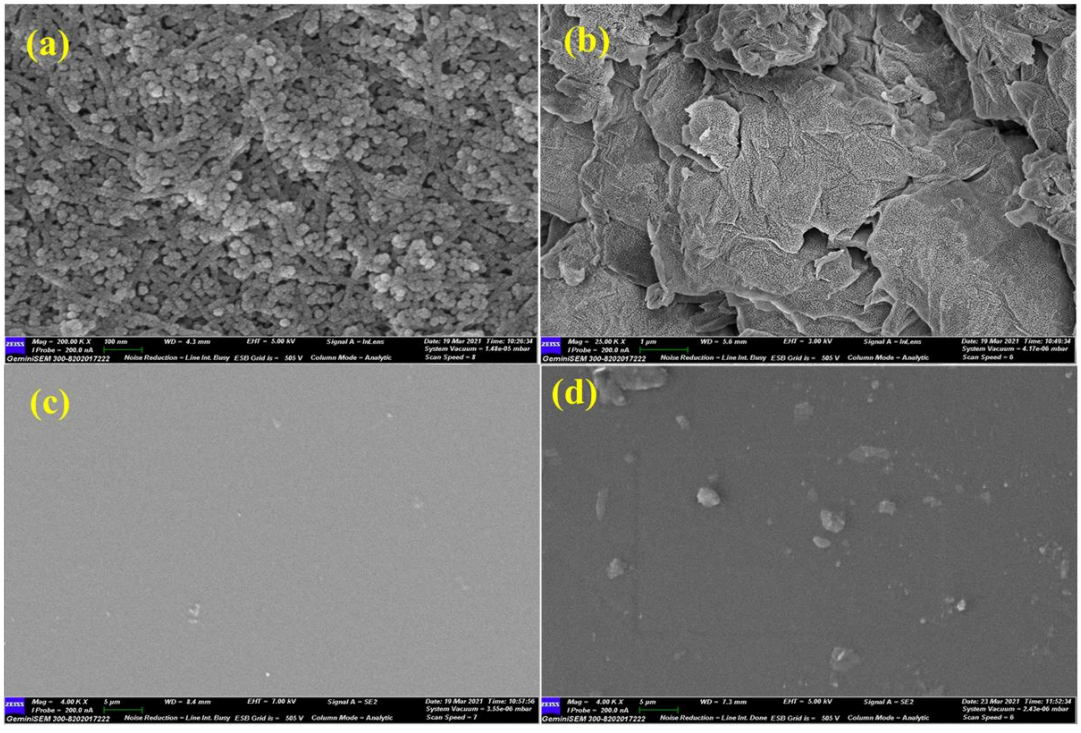

Figure 5. FESEM micrographs of (a) Zinc oxide, (b) graphene oxide, (c) neat chitosan and (d) chitosan/ZnO nanocomposites.

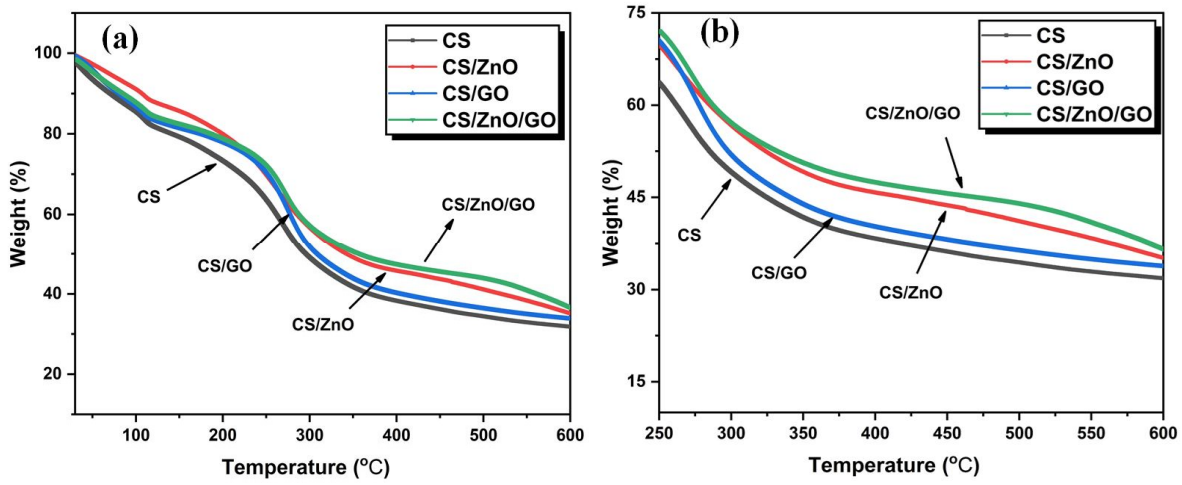

Figure 6. (a) Thermogravimetric (TGA) curves in full temperature range, (b) Expanded view of TGA curve in the temperature range of 250°C to 600°C.

Table 1. Results of thermogravimetric analysis of chitosan and chitosan nanocomposites

Name of Sample	$T_{10\%}$ (°C)	$T_{25\%}$ (°C)	$T_{50\%}$ (°C)
Chitosan	70.5	187.5	295.7
Chitosan/ZnO	107.0	229.0	342.4
Chitosan/GO	80.80	227.0	309.2
Chitosan/ZnO/GO	84.87	234.3	357.76

Note: $T_{5\%}$ - temperature corresponding to 5% weight loss; $T_{50\%}$ − temperature corresponding to 50% weight loss

the temperature for 10 ($T_{10\%}$), 25 ($T_{25\%}$) and 50% ($T_{50\%}$) weight loss are 70.5, 187.5 and 295.7°C respectively. After addition of ZnO nanoparticles (2 wt%) into chitosan film, there is an enhancement of 36.5, 41.5°C and 46.7°C for the $T_{10\%}$, $T_{25\%}$ and $T_{50\%}$ respectively as compared to the neat chitosan. A probable cause leading to the rise in thermal stability of chitosan/ZnO nanocomposites could be due to the hindrance rendered by ZnO nanoparticles to the diffusion of volatiles materials present in chitosan molecules [31]. On the other hand, the enhancement in temperature for $T_{10\%}$, $T_{25\%}$ and $T_{50\%}$ weight loss for chitosan/GO nanocomposites are 10.3, 39.5 and 13.5°C respectively as compared to the neat chitosan. A maximum rise in $T_{25\%}$ and $T_{50\%}$ of 46.5, 62.1°C respectively can be seen for the chitosan/ZnO/GO nanocomposites in comparison to the neat chitosan. This significant rise in thermal stability of hybrid chitosan/ZnO/GO nanocomposites is contributed by the effectual exfoliation of GO and uniform dispersion of ZnO nanofillers into the chitosan matrix. It is also revealed that the interaction of ZnO NPs with the polymer matrix could induce the cross-linking behavior that leads to the rise in thermal stability in the high-temperature range [32]. The DTG (differential thermogravimetric) curves which estimate the rate of thermal decomposition with respect to the temperature of the neat chitosan and chitosan/ZnO/GO nanocomposites are shown in Figure 7. As shown in Figure 7, the maximum decomposition peak for the neat chitosan is 259°C while the peaks for chitosan/ZnO, chitosan/GO and hybrid chitosan/ZnO/GO occurred at 268, 271 and 278°C respectively. Thus, as compared to neat chitosan, the chitosan nanocomposites showed an increase in thermal

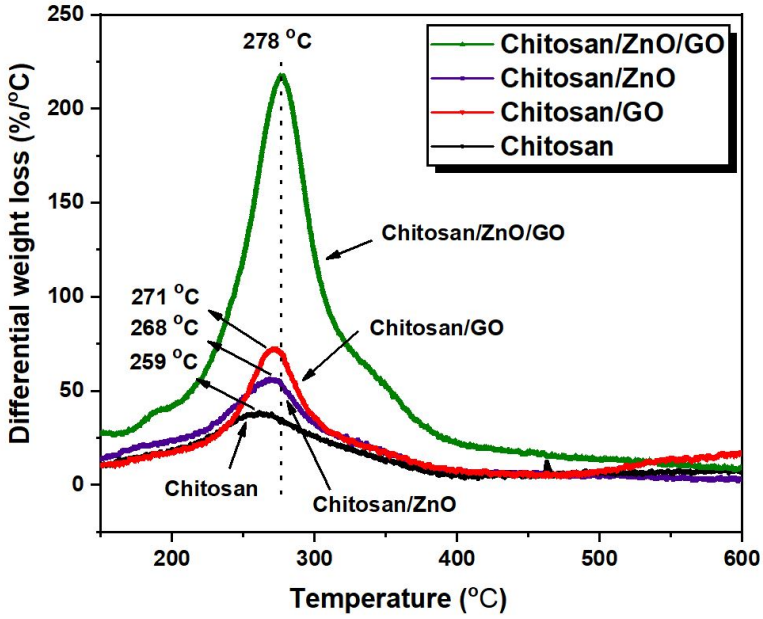

Figure 7. Differential Thermogravimetric (DTG) curves of neat chitosan, chitosan/ZnO, chitosan/GO and chitosan/ZnO/GO nanocomposites.

stability as we have confirmed earlier using TGA curves. The highest inflection point or maximum degradation temperature of 278°C is observed for hybrid chitosan/ZnO/GO nanocomposites which shows marked rise in thermal stability as compared to neat chitosan of 259°C. The results essentially confirm that the addition of hybrid nanofillers offers more resistance to the session of long polymeric chains and resulted in increase of thermal stability.

The water vapor permeability (WVP) which is a measurement of the amount of water that can permeate through the film are analyzed. The results of WVP of neat chitosan and its single and hybrid nanocomposites with ZnO and GO nanofillers can be seen in Figure 8. The WVP of neat chitosan is 2.22 g.mm/m^2.h.kPa. The addition of nanofillers (ZnO, GO and hybrid ZnO/GO) caused a reasonable drop in WVP of final nanocomposites. The nanocomposites of chitosan/ZnO and chitosan/GO after the addition of single nanofillers of ZnO and GO into the chitosan matrix reduced WVP up to 1.38 and 1.34 g.mm/m^2.h.kPa respectively and is almost similar. However, hybrid nanocomposites of chitosan/ZnO/GO showed the minimum WVP of 1.04 g.mm/m^2.h.kPa which is almost 32% lower than single chitosan/ZnO and chitosan/GO nanocomposites. This confirmed that the addition of hybrid nanofillers into the chitosan matrix caused a marked rise in its water barrier properties and that is one of the important properties to protect the food items against microbial contamination. An increase in water barrier properties is essentially attributed to the combined effect of nanofillers which provided the high interatomic interaction between chitosan molecules and ZnO and GO nanofillers.

The results of antibacterial effects of chitosan, chitosan/ZnO, chitosan/GO and hybrid chitosn/ZnO/GO performed in presence of *Bacillus subtilis* (gram-positive bacterium) are shown in Figure 9. The results exhibit variation in the inhibition zone of the neat chitosan and its nanocomposites. The diameter of the inhibition zones as

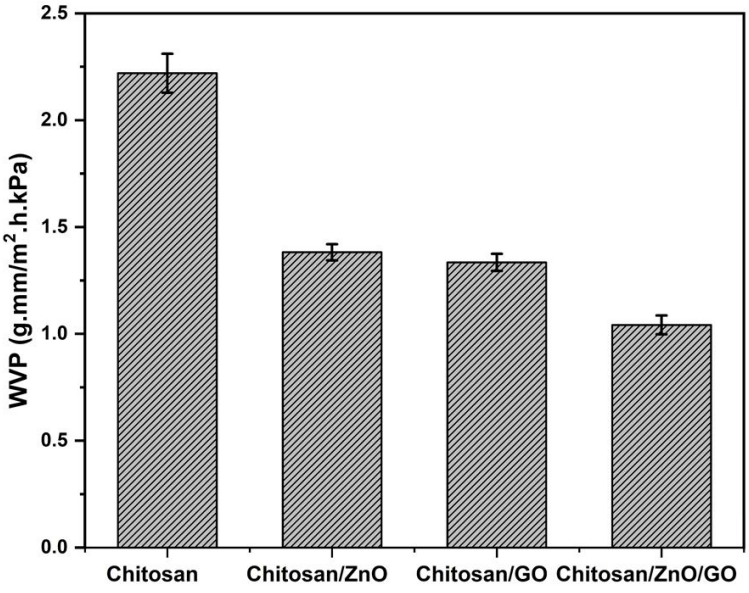

Figure 8. Results ofwater vapor permeability (WVP) of neat chitosan, chitosan/ZnO, chitosan/GO and chitosan/ZnO/GO nanocomposites.

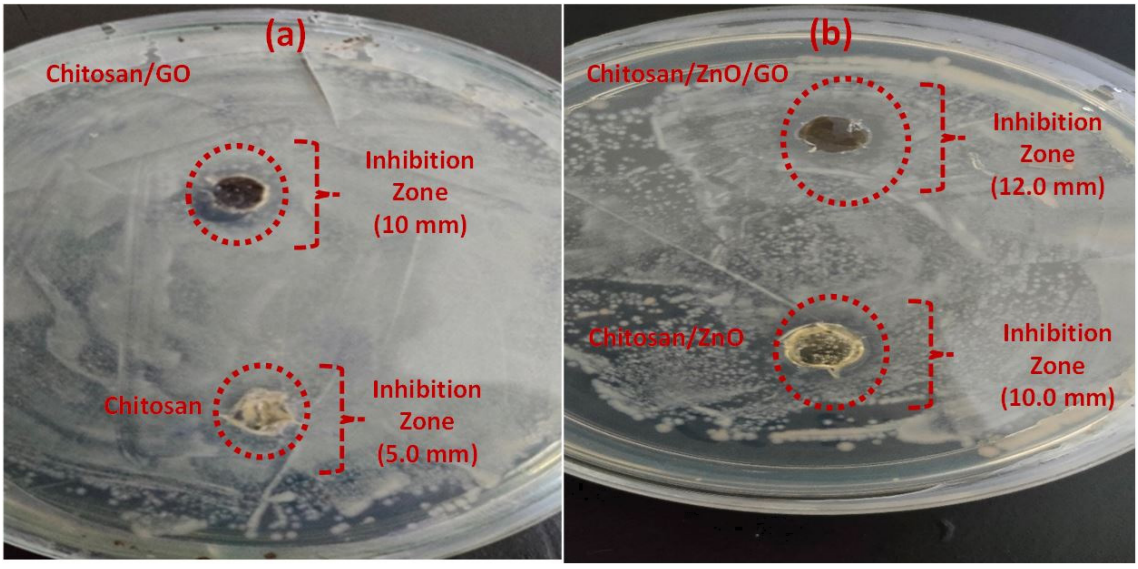

Figure 9. Well diffusion of antibacterial test using *Bacillus subtilis* strain for various samples (a) neat chitosan film and chitosan/GO nanocomposite (b) Chitosan/ZnO and hybrid Chitosan/ZnO/GO nanocomposites.

obtained are as follows: chitosan = 5.0 mm, chitosan/GO = 10.0 mm, chitosan/ZnO = 10.0 mm and hybrid chitosan/ZnO/GO = 12.0 mm. A small value of the inhibition zone of 5.0 mm is observed in neat chitosan due to its intrinsic antibacterial activity against the microorganism as obtained naturally [33]. Addition of single nanofillers of ZnO and GO further increased the inhibition zone and were found the same (10 mm) for both chitosan/ZnO and chitosan/GO nanocomposites. On the other hand, hybrid chitosan/ZnO/GO nanocomposites provided the highest inhibition zone (12.0 mm) as compared to the chitosan/ZnO and chitosan/GO (10.0 mm) as prepared using a single

nanofiller. The above results inferred that the use of hybrid nanofillers of ZnO and GO into chitosan matrix provided more antibacterial activities with enhancement in the inhibition zone as compared to the use of single nanofillers. A similar observation is also found from WVP results where hybrid chitosan/ZnO/GO showed minimum WVP as compared to the chitosan/ZnO and chitosan/GO nanocomposites.

Conclusion

The effects of single and hybrid nanofillers in the preparation of chitosan nanocomposites for the evaluation of various physical properties (thermal, water vapor barrier, and antimicrobial) were investigated. The results showed a significant rise in thermal stability of hybrid chitosan/ZnO/GO nanocomposites as compared to the neat chitosan and chitosan/ ZnO and chitosan/GO nanocomposites. The addition of hybrid nanofillers increased the resistance to the volatile materials and strengthen the intermolecular bond structures between the cellulosic compounds. Also, a marked reduction in water vapor permeation (WVR) was observed in hybrid nanocomposites as compared to neat chitosan and chitosan nanocomposites prepared with single nanofillers of ZnO and GO. A high inhibition zone formed around the film of hybrid chitosan/ZnO/GO nanocomposites further revealed the advantageous effect of hybrid nanocomposites and could be used as an antibacterial agent in food packaging materials. The outstanding physical properties of hybrid nanocomposites were ascribed due to the successful transfer of their characteristics into the chitosan matrix with uniform dispersion.

References

[1] D.K.A. Barnes, F. Galgani, R.C. Thompson, and M. Barlaz, *Accumulation and fragmentation of plastic debris in global environments.* Philosophical Transactions of the Royal Society B: Biological Sciences. 364(1526) (2009), pp. 1985-1998.

[2] M. Flury and R. Narayan, *Biodegradable plastic as an integral part of the solution to plastic waste pollution of the environment.* Current Opinion in Green and Sustainable Chemistry. 30 (2021), pp. 1-7.

[3] L.S. Dilkes-Hoffman, S. Pratt, P.A. Lant, and B. Laycock, *The Role of Biodegradable Plastic in Solving Plastic Solid Waste Accumulation.* Plastics to Energy. (2019), pp. 469-505.

[4] S. Bandopadhyay, L. Martin-Closas, A.M. Pelacho, and J.M. DeBruyn, *Biodegradable Plastic Mulch Films: Impacts on Soil Microbial Communities and Ecosystem Functions.* Frontiers in Microbiology. 9 (2018).

[5] T. Morohoshi, T. Oi, H. Aiso, T. Suzuki, T. Okura, and S. Sato, *Biofilm Formation and Degradation of Commercially Available Biodegradable Plastic Films by Bacterial Consortiums in Freshwater Environments.* Microbes and Environments. 33(3) (2018), pp. 332-335.

[6] M. de Morais Lima, L.C. Carneiro, D. Bianchini, A.R.G. Dias, E. da Rosa Zavareze, C. Prentice, and A. da Silveira Moreira, *Structural, Thermal, Physical, Mechanical, and Barrier Properties of Chitosan Films with the Addition of Xanthan Gum.* Journal of Food Science. 82(3) (2017), pp. 698-705.

[7] F.K.G. dos Santos, K.N. de O. Silva, T.D.N. Xavier, R.H. de L. Leite, and E.M.M. Aroucha, *Effect of the Addition of Carnauba Wax on Physicochemical Properties of Chitosan Films.* Materials Research. 20(2) (2017), pp. 479-484.

[8] F. Luangapai, M. Peanparkdee, and S. Iwamoto, *Biopolymer films for food industries: properties, applications, and future aspects based on chitosan.* Reviews in Agricultural Science. 7 (2019), pp. 59-67.

[9] G.S. Dhillon, S. Kaur, and S.K. Brar, *Facile fabrication and characterization of chitosan-based zinc oxide nanoparticles and evaluation of their antimicrobial and antibiofilm activity.* International Nano Letters. 4(2) (2014), p. 107.

[10] B. Nowack, H.F. Krug, and M. Height, *120 Years of Nanosilver History: Implications for Policy Makers.* Environmental Science & Technology. 45(4) (2011), pp. 1177-1183.

[11] Y. Echegoyen and C. Nerín, *Nanoparticle release from nano-silver antimicrobial food containers.* Food and Chemical Toxicology. 62 (2013), pp. 16-22.

[12] G. Applerot, A. Lipovsky, R. Dror, N. Perkas, Y. Nitzan, R. Lubart, and A. Gedanken, *Enhanced Antibacterial Activity of Nanocrystalline ZnO Due to Increased ROS-Mediated Cell Injury.* Advanced Functional Materials. 19(6) (2009), pp. 842-852.

[13] T. Naseem and T. Durrani, *The role of some important metal oxide nanoparticles for wastewater and antibacterial applications: A review.* Environmental Chemistry and Ecotoxicology. 3 (2021), pp. 59-75.

[14] P. Terzioglu, Y. Altin, A. Kalemtas, and A. Celik Bedeloglu, *Graphene oxide and zinc oxide decorated chitosan nanocomposite biofilms for packaging applications*. Journal of Polymer Engineering. 40(2) (2020), pp. 152-157. DOI: 10.1515/polyeng-2019-0240.

[15] A. Giannakas, P. Stathopoulou, G. Tsiamis, and C. Salmas, *The effect of different preparation methods on the development of chitosan/thyme oil/montmorillonite nanocomposite active packaging films*. Journal of Food Processing and Preservation. 44(2) (2019), pp. 1-15.

[16] W. Yang, E. Fortunati, F. Bertoglio, J. Owczarek, G. Bruni, M. Kozanecki, J. Kenny, L. Torre, L. Visai, and D. Puglia, *Polyvinyl alcohol/chitosan hydrogels with enhanced antioxidant and antibacterial properties induced by lignin nanoparticles.* Carbohydrate Polymers. 181 (2018), pp. 275-284.

[17] R. Priyadarshi and Y.S. Negi, *Effect of Varying Filler Concentration on Zinc Oxide Nanoparticle Embedded Chitosan Films as Potential Food Packaging Material.* Journal of Polymers and the Environment. 25(4) (2017), pp. 1087-1098.

[18] S. Valizadeh, M. Naseri, S. Babaei, S.M.H. Hosseini, and A. Imani, *Development of bioactive composite films from chitosan and carboxymethyl cellulose using glutaraldehyde, cinnamon essential oil and oleic acid.* International Journal of Biological Macromolecules. 134 (2019), pp. 604-612.

[19] S. Shankar and J.W. Rhim, *Preparation of sulfur nanoparticle-incorporated antimicrobial chitosan films.* Food Hydrocolloids. 82 (2018), pp. 116-123.

[20] A. Vishwakarma, *Synthesis of Zinc Oxide Nanoparticle by Sol-Gel Method and Study its Characterization.* International Journal for Research in Applied Science and Engineering Technology. 8(4) (2020), pp. 1625-1627.

[21] D.C. Marcano, D.V. Kosynkin, J.M. Berlin, A. Sinitskii, Z. Sun, A. Slesarev, L.B. Alemany, W. Lu, and J.M. Tour, *Improved Synthesis of Graphene Oxide.* ACS Nano. 4(8) (2010), pp. 4806-4814.

[22] V. Guillard, B. Broyart, C. Bonazzi, S. Guilbert, and N. Gontard, *Preventing Moisture Transfer in a Composite Food Using Edible Films: Experimental and Mathematical Study.* Journal of Food Science. 68(7) (2003), pp. 2267-2277.

[23] M.R. Martelli, T.T. Barros, M.R. de Moura, L.H.C. Mattoso, and O.B.G. Assis, *Effect of Chitosan Nanoparticles and Pectin Content on Mechanical Properties and Water Vapor Permeability of Banana Puree Films.* Journal of Food Science. 78(1) (2013), pp. N98-N104.

[24] M.K. Poddar, S. Pradhan, V.S. Moholkar, M. Arjmand, and U. Sundararaj, *Ultrasound-assisted synthesis and characterization of polymethyl methacrylate/reduced graphene oxide nanocomposites.* AIChE Journal. 64(2)

(2018), pp. 673-687.

[25] S. Perumbilavil, P. Sankar, T. Priya Rose, and R. Philip, *White light Z-scan measurements of ultrafast optical nonlinearity in reduced graphene oxide nanosheets in the 400-700 nm region.* Applied Physics Letters. 107(5) (2015), pp.1-5.

[26] U. Siripatrawan and B.R. Harte, *Physical properties and antioxidant activity of an active film from chitosan incorporated with green tea extract.* Food Hydrocolloids. 24(8) (2011), pp. 770-775.

[27] J. Brugnerotto, J. Lizardi, F.M. Goycoolea, W. Argüelles-Monal, J. Desbrières, and M. Rinaudo, *An infrared investigation in relation with chitin and chitosan characterization.* Polymer. 42(8) (2001), pp. 3569-3580.

[28] Y. Haldorai and J.J. Shim, *Chitosan-Zinc Oxide hybrid composite for enhanced dye degradation and antibacterial activity*. Composite Interfaces. 20(5) (2013), pp. 365-377.

[29] M. Lavorgna, F. Piscitelli, P. Mangiacapra, and G.G. Buonocore, *Study of the combined effect of both clay and glycerol plasticizer on the properties of chitosan films.* Carbohydrate Polymers. 82(2) (2010), pp. 291-298.

[30] F.S. Kittur, A.B. Vishu Kumar, and R.N. Tharanathan, *Low molecular weight chitosans—preparation by depolymerization with Aspergillus niger pectinase, and characterization.* Carbohydrate Research. 338(12) (2003), pp. 1283-1290.

[31] S. Kumar, B. Krishnakumar, A.J.F.N. Sobral, and J. Koh, *Bio-based (chitosan/PVA/ZnO) nanocomposites film: Thermally stable and photoluminescence material for removal of organic dye.* Carbohydrate Polymers. 205 (2019), pp. 559-564.

[32] M.K. Poddar, S. Sharma, and V.S. Moholkar, *Investigations in two-step ultrasonic synthesis of PMMA/ZnO nanocomposites by in-situ emulsion polymerization.* Polymer. 99 (2016), pp. 453-469.

[33] H.Y. Atay, *Antibacterial Activity of Chitosan-Based Systems*. Functional Chitosan. (2019), pp. 457-489.